

One-step Hydrothermal Synthesis of Ultralow Pt Loading Ni(OH)₂ for Enhanced Hydrogen Evolution Reaction

Jiao Chen¹, Hongye Qin¹, Yaping Pan¹, Jinli Wu¹, Jianan Liu¹, Wanying Lin¹, Jun Jiang¹, Enzuo Liu^{1,2}, Junwei Sha¹, Fang He¹, Liying Ma^{1,*}, Naiqin Zhao^{1,2,3}

¹ School of materials science and engineering and Tianjin Key Laboratory of Composites and Functional Materials, Tianjin University, Tianjin 300350, China

² Collaborative Innovation Center of Chemical Science and Engineering, Tianjin 300350, China

³ Key Laboratory of Advanced Ceramics and Machining Technology, Ministry of Education, Tianjin, 300350, China

*E-mail: lyma@tju.edu.cn

Received: 9 March 2021 / Accepted: 4 May 2021 / Published: 31 May 2021

It is necessary and challenging to develop platinum-based electrocatalysts with low Pt content and high performance for industrial development in a suitable strategy. Herein, ultralow Pt (0.35 wt%) loading Ni(OH)₂ nanosheets (named as 2-Pt/Ni(OH)₂) with cataphracted structure is synthesized on nickel foam by one-step hydrothermal process. It only needs an overpotential of 34 mV to achieve a current density of 10 mA cm⁻² without any significant decrease for 40 hours. This excellent performance of hydrogen evolution reaction (HER) is attributed to the fact that the cataphracted structure not only has a larger active area and more active sites, but also effectively limits the size of Pt nanoparticles to 2~3 nm, which results in a higher active quality. In addition, the relatively simple and easily operational one-step method can reduce the Pt content to 0.35 wt% significantly. This facile strategy opens up new approaches in the rational design and synthesis of low loading Pt electrocatalysts with eminent electrocatalytic activity for industrial production.

Keywords: Pt/Ni(OH)₂, hydrothermal method, cataphracted structure, hydrogen evolution reaction

1. INTRODUCTION

To solve the problems of environmental pollution and energy shortage, researchers have made great efforts to develop clean, renewable and sustainable energy [1-3]. Compared with some intermittent energy sources such as wind, solar and tidal power which can be easily affected by the natural environment [4, 5], hydrogen holds great promise because of its environmentally friendly and storable characteristics [6, 7]. Furthermore, alkaline water electrolysis with high quality and non-pollution has been considered as a highly promising approach for abundant hydrogen production [8, 9]. To improve

the efficiency of water electrolysis, designing electrocatalysts with excellent performance is necessary.

Currently, platinum (Pt) and Pt-based catalysts are recognized as state-of-the-art catalytic materials for the HER, attributed to the strong ability to adsorb and recombine reactive hydrogen intermediates for efficient water molecule adsorption [10]. However, high cost and poor stability limited its industrial application [11, 12]. Although other non-Pt materials are rich in resources and low in cost [13-15], their high overpotential and high energy consumption greatly limit the use of HER. Constructing heterojunction is one of the most effective methods to improve the properties of electrocatalysts, which can adjust the electronic structure and change the adsorption and desorption energy of the intermediate on the catalyst surface [16, 17]. Therefore, combining an extremely small amount of Pt with non-precious metal materials to construct heterogeneous structural materials is expected to be an effective way to prepare catalysts with enhanced activity, strong stability and low cost.

Among non-precious metals, nickel hydroxide ($\text{Ni}(\text{OH})_2$) stands out because of the enhanced H_2O cleavage and OH^- adsorption during HER process [18-20]. Therefore, $\text{Ni}(\text{OH})_2$ combined with Pt is an excellent candidate to construct electrocatalysts [21-23]. As reported, Xiao *et al.* raised the loading of alpha- or beta-nickel hydroxide (α or β - $\text{Ni}(\text{OH})_2$) nanostructures on the surface of Pt electrode to improve its catalytic activity and stability for HER [24]. William C *et al.* reported the design, synthesis and exceptional performance of 3D biotemplated Pt- $\text{Ni}(\text{OH})_2$ nanonetworks in alkaline HER electrocatalysis [25]. However, there are still some problems to be further improved in the construction of Pt- $\text{Ni}(\text{OH})_2$ catalyst. On one hand, some Pt- $\text{Ni}(\text{OH})_2$ electrocatalysts still have high Pt content and thus achieve high performance similar to Pt/C [26, 27], which makes it difficult to reduce costs. On the other hand, some synthesis methods of Pt- $\text{Ni}(\text{OH})_2$ require strict physical or chemical conditions [28], which still limit their industrial application. Hence, designing a simple method to develop high-performance Pt- $\text{Ni}(\text{OH})_2$ electrocatalysts with ultralow Pt content for alkaline HER is an urgent need and a huge challenge.

Herein, we prepared ultralow Pt (0.35 wt%) loading cataphracted $\text{Ni}(\text{OH})_2$ nanosheets (2-Pt/ $\text{Ni}(\text{OH})_2$) by a controllable and low-cost one-step hydrothermal method. Experiments and theories proved that the enhanced HER performance of 2-Pt/ $\text{Ni}(\text{OH})_2$ is attributed to the cataphracted structure. H^+ from H_2PtCl_6 led to the formation of small nanosheets (~150 nm) of Pt/ $\text{Ni}(\text{OH})_2$, which is in favor of more exposed $\text{Ni}(\text{OH})_2$ edges to greatly promote the hydrolysis and improve the reaction kinetics. Besides, the metal Ni derived from nickel foam (NF) was reduced Pt^{4+} (PtCl_4^{2-} from H_2PtCl_6) to Pt^0 through an oxidation-reduction reaction and the size of Pt nanoparticles (NPs) was limited to 2~3 nm, which can effectively expose the contact area of the active site and thus boost the hydrogen production as a result. The developed one-step hydrothermal method greatly improves the Pt utilization and reduces the production cost, which provides not only a cost-effective and highly active Pt- $\text{Ni}(\text{OH})_2$ electrocatalyst, but also a novel idea for the heterojunction construction.

2. EXPERIMENTS

2.1. Materials

All chemicals were applied as received without further purification. Nickel foam (NF) with a thickness of 2 mm was provided by Jiashide Foam Metal Co., Ltd.. Nickel nitrate hexahydrate

($\text{Ni}(\text{NO}_3)_2 \cdot 6\text{H}_2\text{O}$, Adamas Reagent), urea ($\text{CH}_4\text{N}_2\text{O}$, Aladdin Co., Ltd.) and ammonium fluoride (NH_4F , Aladdin Co., Ltd.) were used to obtain $\text{Ni}(\text{OH})_2$. Chloroplatinic acid (H_2PtCl_6 , Aladdin Co., Ltd.) was selected as Pt source to synthesize $\text{Pt}/\text{Ni}(\text{OH})_2$. Pt/C (20 wt% Pt) was purchased from Hesen Co. Ltd. Nafion (5 wt%) was bought from Sigma-Aldrich Chemical Reagent Co., Ltd.

2.2. Synthesis

2.2.1 Synthesis of $\text{Pt}/\text{Ni}(\text{OH})_2$ on Nickel Foam

NF (1 cm \times 3 cm) was used as the substrate for hydrothermal synthesis. To remove the surface oxide layer, NF was cleaned by ultrasonication in acetone and subsequently 3 M HCl for 15 min, then rinsed with deionized water and absolute ethanol in turn and dried in an electric vacuum. 0.6 mmol $\text{Ni}(\text{NO}_3)_2 \cdot 6\text{H}_2\text{O}$, 3 mmol $\text{CH}_4\text{N}_2\text{O}$, 1.5 mmol NH_4F and H_2PtCl_6 (0 mmol, 0.001 mmol, 0.01 mmol and 0.03 mmol) were dissolved in 20 mL of deionized water and stirred for at least 20 min to form a light green solution. The homogeneous solution was transferred into a 50 mL Teflon-lined stainless steel autoclave, and the cleaned NF was immersed into the vessel, which was kept at 120°C for 8 h. After that, the autoclave was quickly cooled down by water. The NF was taken out and carefully rinsed with deionized water and absolute ethanol several times with the assistance of ultrasonication. The obtained samples were named $\text{Ni}(\text{OH})_2$, 1-Pt/ $\text{Ni}(\text{OH})_2$, 2-Pt/ $\text{Ni}(\text{OH})_2$ and 3-Pt/ $\text{Ni}(\text{OH})_2$.

2.2.2 Synthesis of *c*- $\text{Ni}(\text{OH})_2$, *c*-Pt/ $\text{Ni}(\text{OH})_2$ and *t*-Pt/ $\text{Ni}(\text{OH})_2$ on Nickel Foam

In order to verify and eliminate the effect of H^+ on hydrogen evolution performance, a controlled experiment similar to the $\text{Ni}(\text{OH})_2$ synthesis process was prepared. Except for the reactants of $\text{Ni}(\text{OH})_2$, HCl was added in one-step hydrothermal process. Finally the product was referred to *c*- $\text{Ni}(\text{OH})_2$. The preparation of another controlled experiment was in contrast to that of Pt/ $\text{Ni}(\text{OH})_2$. Except for the reactants of Pt/ $\text{Ni}(\text{OH})_2$, NH_4OH was added to make the solution neutral in one-step hydrothermal process. And the product was called as *c*-Pt/ $\text{Ni}(\text{OH})_2$.

Besides, the two-step hydrothermal method was adopted as a contrast to prove the superiority of one-step hydrothermal method. Firstly, the previous steps were followed to obtain $\text{Ni}(\text{OH})_2$. Then, $\text{Ni}(\text{OH})_2$, 0.01 mmol H_2PtCl_6 and 20 mL of deionized water were transferred into a 50 mL Teflon-lined stainless steel autoclave which was kept at 120°C for 8 h. After quickly cooled down by water, the obtained product was named as *t*-Pt/ $\text{Ni}(\text{OH})_2$.

2.3. Materials characterizations

Scanning electron microscopy (SEM) images were acquired by Hitachi S4800 scanning microscope. Transmission electron microscopy (TEM) images and energy dispersive X-ray spectrum (EDS) mapping were obtained from JEOL JEM-2010 at 200 kV. X-ray diffraction (XRD) characterizations were performed on a DX-2700BH Advance diffractometer operating with monochro-

mated Cu Ka radiation in the 2θ range from 10° to 90° . The surface composition and valence state were analyzed by X-ray photoelectron spectroscopy (XPS, Thermo ESCALAB 250XI). All XPS spectra were calibrated by shifting the detected adventitious carbon C 1s peak to 284.8 eV.

2.4. Electrochemical characterizations

The electrochemical measurements were performed with a CHI 760E electrochemistry workstation in a three-electrode system. A Hg/HgO electrode and a carbon rod were applied as the reference counter electrode. The samples ($0.5\text{ cm} \times 0.5\text{ cm}$) were directly used as the working electrode. The electrolyte of 1 M KOH with Ar saturated was used for the HER tests. The polarization curves were obtained by linear sweep voltammetry (LSV) at a scan rate 5 mV s^{-1} . The electrochemically active surface area (ECSA) was estimated from the electrochemical double-layer capacitance (C_{dl}) in a non-Faradaic region (0.767 to 0.967 V vs. RHE).

3. RESULTS AND DISCUSSION

3.1 SEM and TEM Analysis of Pt/Ni(OH)₂

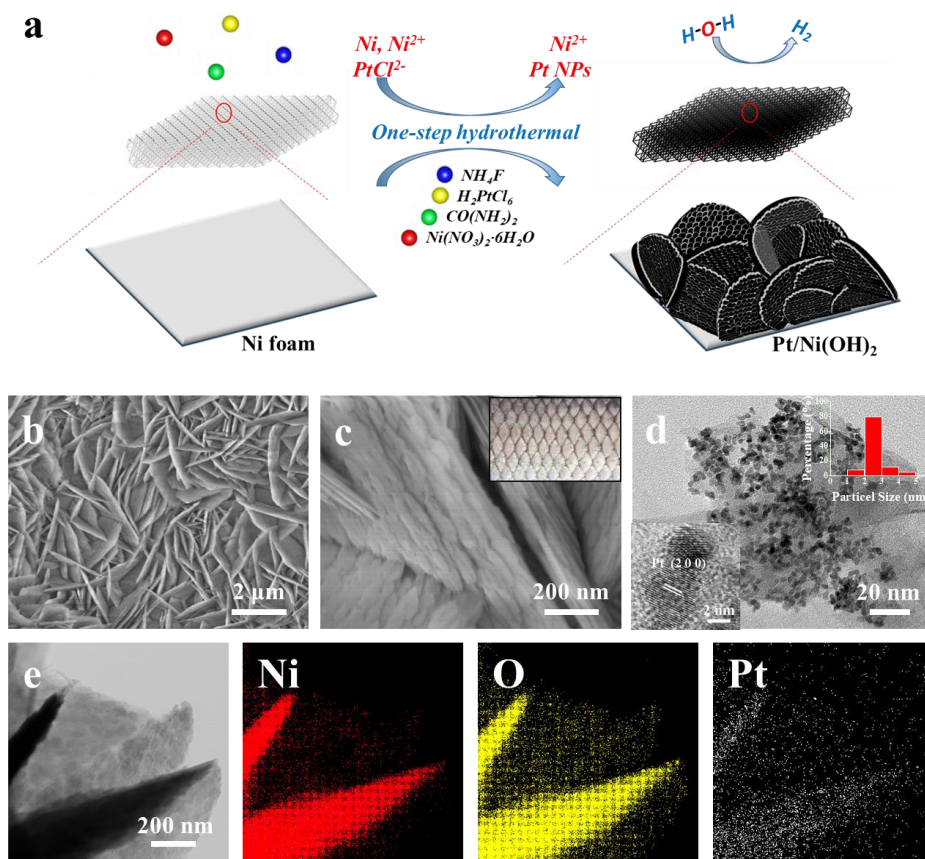


Figure 1. (a) Schematic diagram of Pt/Ni(OH)₂ for HER. (b) Low-magnification SEM image of 2-Pt/Ni(OH)₂. (c) High-magnification SEM image of 2-Pt/Ni(OH)₂. The inset shows a picture of fish scale. (d) TEM image of 2-Pt/Ni(OH)₂. The size distribution of Pt nanoparticles and HRTEM image of 2-Pt/Ni(OH)₂ are shown in the two insets, respectively. (e) STEM image and the corresponding elemental mappings of Ni, O, and Pt of 2-Pt/Ni(OH)₂.

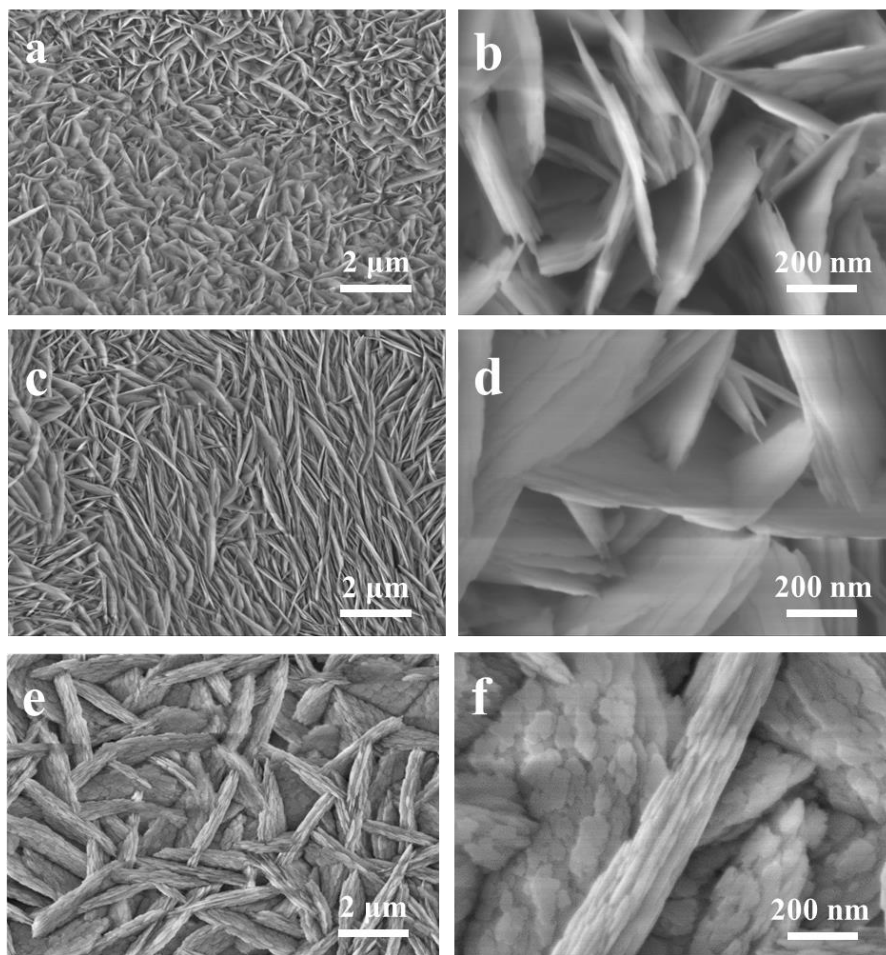


Figure 2. (a, c and e) Low-magnification and (b, d and f) high-magnification SEM images of Ni(OH)₂, 1-Pt/Ni(OH)₂ and 3-Pt/Ni(OH)₂.

The synthesis process of Pt/Ni(OH)₂ is illustrated in Figure 1a. Pt NPs were successfully loaded on Ni(OH)₂ nanosheets with cataphracted morphology by one-step hydrothermal method. The morphological structure of the composite was characterized using scanning electron microscopy (SEM) and transmission electron microscopy (TEM). Figure 1b presents representative SEM images of 2-Pt/Ni(OH)₂ indicating that the nanosheets with large interlayer clearance grow vertically on NF, which is conducive to charge transfer and ion-permeable behavior [29]. The larger nanosheets are all covered by smaller nanosheets with a diameter of about 150 nm, which were called cataphracted nanosheets. The SEM images of Pt/Ni(OH)₂ electrocatalysts with different Pt contents are shown in Figure 2. With the increase of Pt content, both the length and thickness of Pt/Ni(OH)₂ nanosheets increased. Among them, it is obvious that 2-Pt/Ni(OH)₂ are the most neatly arranged and evenly distributed, which leads to the exposure of more Ni(OH)₂ edges. In addition, when the content of H₂PtCl₆ in the reactants is too low, the cataphracted morphology cannot be formed; when the content is too high, the morphology can be destroyed easily. The average size of Pt NPs in 2-Pt/Ni(OH)₂ electrocatalysts was 2~3 nm (see Figure 1c), showing higher quality activity and better durability [30]. The high-resolution TEM (HRTEM) image of 2-Pt/Ni(OH)₂ in Figure S2 reveals the well-resolved lattice fringes with an interplanar distance

of 0.139 nm which corresponding to the (220) plane Pt. Moreover, elemental mapping further demonstrates the homogenous distribution of Ni, O, and Pt throughout the nanosheet structure in 2-Pt/Ni(OH)₂ (Figure 1e). Therefore, the Pt NPs with the size of 2~3 nm were successfully loaded on Ni(OH)₂ nanosheets which forming the unique cataphracted structure.

3.2 XRD and ICP Analysis of Pt/Ni(OH)₂

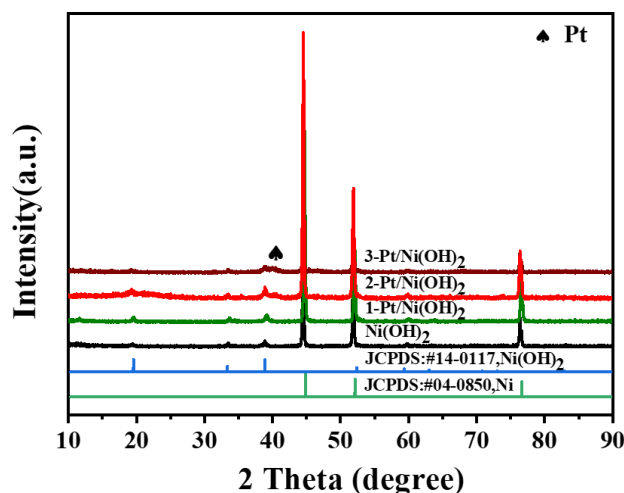


Figure 3. (a) XRD pattern of Ni(OH)₂, 1-Pt/Ni(OH)₂, 2-Pt/Ni(OH)₂ and 3-Pt/Ni(OH)₂.

Figure 3 shows X-ray diffraction (XRD) patterns of the prepared Pt/Ni(OH)₂ samples. Obviously, the diffraction peaks of all samples are well correlated with the patterns of metallic Ni (JCPDS:#04-0850) and Ni(OH)₂ (JCPDS:#14-0117). Due to the content of Pt is too low, the characteristic peak of Pt can not be found in Figure 2a [31, 32]. With the loading amount of Pt increased, the characteristic peak of Pt appears in the XRD pattern of 3-Pt/Ni(OH)₂ which reflects the successful loading of Pt on Ni(OH)₂.

According to an inductively coupled plasma mass spectrometry (ICP-MS) technique, the Pt content in 1-Pt/Ni(OH)₂, 2-Pt/Ni(OH)₂ and 3-Pt/Ni(OH)₂ is quantitatively measured at 0.05 wt%, 0.35 wt% and 1.65 wt% in Table 1. The Pt content of the prepared Pt/Ni(OH)₂ samples is much lower than most Pt-based materials (see Table 2). In a word, the one-step hydrothermal method has successfully reduced the Pt content to a new level and greatly improved the utilization rate of Pt.

Table 1. The inductively coupled plasma measurement (ICP) results for 1-Pt/Ni(OH)₂, 2-Pt/Ni(OH)₂ and 3-Pt/Ni(OH)₂.

Sample	Mass fraction of Pt in Pt/Ni(OH) ₂ (wt%)
1-Pt/Ni(OH) ₂	0.05%
2-Pt/Ni(OH) ₂	0.35%
3-Pt/Ni(OH) ₂	1.65%

Table 2. Comparison of HER performance for Pt/Ni(OH)₂ with other Pt-based electrocatalysts in 1 M KOH.

Catalyst	Overpotentials (mV, at 10 mA cm ⁻²)	Pt content (wt %)	Ref.
Pt/Ni(OH) ₂	34	0.35	This work
0.45%Pt–Ni ₃ N/Ni@C	45	0.49	[33]
Ni(OH) ₂ -PtO ₂ NS/Ti	> 45	5.10	[34]
Pt1-Mo ₂ C-C	155	0.70	[35]
Ni ₃ N/Pt	50	15.00	[27]
Pt NWs/SL-Ni(OH) ₂	> 85	38.00	[36]
β-Ni(OH) ₂ /Pt	75	Pt electrode	[24]

3.3 XPS Analysis of Pt/Ni(OH)₂

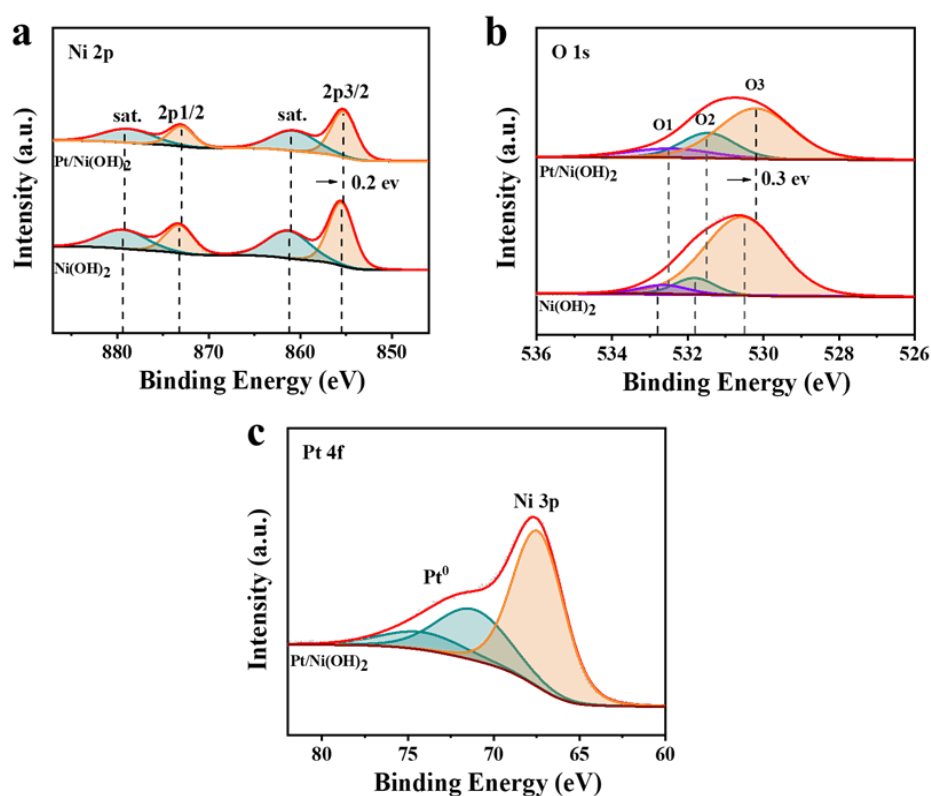
**Figure 4.** XPS spectra in the (a) Ni 2p, (b) Pt 4f for Ni(OH)₂ and 2-Pt/Ni(OH)₂ and (c) Pt 4f for 2-Pt/Ni(OH)₂.

Figure 4a and 4b show the high-resolution XPS spectra of Ni 2p and O 1s for Ni(OH)₂ and Pt-Ni(OH)₂, respectively. In the Ni 2p XPS spectra of 2-Pt-Ni(OH)₂, the binding energies (BEs) at 873.0, 855.3, 879.2 and 861.0 eV can be assigned to Ni 2p_{1/2}, Ni 2p_{3/2} and their satellite peak [37, 38], which negatively shifting 0.2 eV to that of Ni(OH)₂. In the O 1s XPS spectra, the BEs at 532.5, 531.5 and 530.2 eV (marked O1, O2, O3) can correspond to the adsorbed water, the Ni-(OH) bond and the metal-bond in Ni(OH)₂ [34], which negatively shifting 0.3 eV to that of Ni(OH)₂. In Figure 4c, the BEs of Pt/Ni(OH)₂

at 74.8 and 71.4 eV just positive shift at about 0.4 eV than the price state of metallic Pt, which will lead to the down-shift of Pt d-band center and enhance the HER performance [39-40]. And a Ni 3p peak coexists in the Pt 4f XPS spectra which is ascribed to Ni²⁺ species in Ni(OH)₂. Well consistent with TEM results, the XPS result indicates the presence of Ni(OH)₂ and Pt. Besides, Ni 2p and O 1s peak of Pt/Ni(OH)₂ are both red-shifted relative to Ni(OH)₂ and Pt 4f peak of Pt/Ni(OH)₂ is blue-shifted relative to metallic Pt, which suggests a strong interaction between Pt and Ni(OH)₂ [41].

3.4 Electrochemical Performance of Pt/Ni(OH)₂

Electrochemical measurements about Ni(OH)₂, 1-Pt/Ni(OH)₂, 2-Pt/Ni(OH)₂, 3-Pt/Ni(OH)₂ and Pt/C were examined in a typical three-electrode system using 1 M KOH solution as electrolyte. The linear sweep voltammetry (LSV) curves in Figure 5a show the overpotentials of Ni(OH)₂, 1-Pt/Ni(OH)₂, 2-Pt/Ni(OH)₂, 3-Pt/Ni(OH)₂ and Pt/C are 216, 55, 34, 45 and 40 mV at the current density of 10 mA cm⁻², representely. Compared with Ni(OH)₂, all Pt/Ni(OH)₂ samples show a significant improvement in HER performance and 2-Pt/Ni(OH)₂ has the optimal HER activity even superior to Pt/C electrode. Besides, 2-Pt/Ni(OH)₂ only needs the lowest overpotential (92 and 148 mV) to get the current density of 50 and 100 mA cm⁻² which indicates 2-Pt/Ni(OH)₂ has a faster hydrogen precipitation rate. In Figure 5b, the Tafel slope of 2-Pt/Ni(OH)₂ (42 mV dec⁻¹) is much smaller than that of Ni(OH)₂ (121 mV dec⁻¹), 1-Pt/Ni(OH)₂ (70 mV dec⁻¹) and 3-Pt/Ni(OH)₂ (53 mV dec⁻¹), which means that 2-Pt/Ni(OH)₂ has a faster HER rate and positive catalytic kinetics [42]. For 2-Pt/Ni(OH)₂, the HER kinetic behavior can be allocated to the Volmer-Heyrovsky mechanism, suggesting that the synergistic interaction between Ni(OH)₂ and Pt can promote both water dissociation and H₂ release [43, 44]. Besides, the electrochemical impedance spectroscopy (EIS) results display the charge transfer resistance (*R*_{ct}) of the prepared samples in Figure 5c. The *R*_{ct} value of 2-Pt/Ni(OH)₂ is lower than that of other samples, indicating that 2-Pt/Ni(OH)₂ has excellent electrical conductivity and faster electron transfer kinetics [6, 45]. Consequently, the above results show that 2-Pt/Ni(OH)₂ has the best HER performance compared to other samples.

Stability is also an important criterion for electrocatalysts. Figure 5d shows long-term stability of 2-Pt/Ni(OH)₂ at a constant overpotential of 34 mV. The performance of 2-Pt/Ni(OH)₂ is hardly observed degradation and the morphology can still maintain the original structure even after the 40-hour stability test. Delightedly, the stability of 2-Pt/Ni(OH)₂ precedes most Pt-based electrocatalysts [46-49]. This excellent stability is attributed to the close combination between Pt nanoparticles and Ni(OH)₂ nanosheets synthesized by one-step hydrothermal method. In a word, 2-Pt/Ni(OH)₂ is a remarkable activity and strong stability HER catalyst with ultra-high Pt utilization, which presumably due to its cataphracted structure.

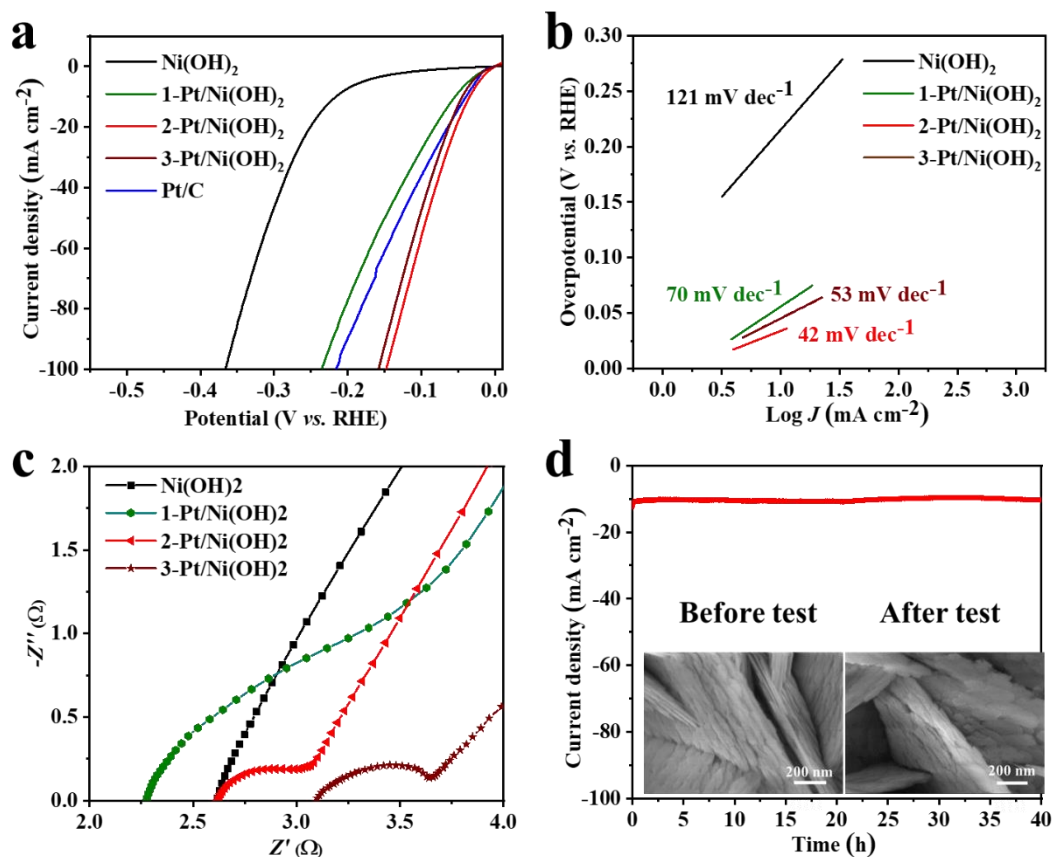


Figure 5. Electrocatalytic HER performance of Ni(OH)₂, 1-Pt/Ni(OH)₂, 2-Pt/Ni(OH)₂ and Pt/C in 1 M KOH electrolyte. (a) LSV curves without iR correction at a sweep rate of 5 mV s⁻¹. (b) Tafel plots. (c) Nyquist plots. (d) Current density versus time curves of Pt/Ni(OH)₂ recorded for 40 h at 10 mA cm⁻² vs. RHE; SEM images of 2-Pt/Ni(OH)₂ before and after 40 h stability test are illustrated in the insets.

3.5 SEM Analysis of *c*-Ni(OH)₂, *c*-Pt/Ni(OH)₂, *t*-Pt/Ni(OH)₂

In order to further study 2-Pt/Ni(OH)₂ cataphracted structure, we took Ni(OH)₂ and 2-Pt/Ni(OH)₂ (also simply called Pt/Ni(OH)₂) as references to conduct corresponding controlled tests. Since NH₄F was used to limit the growth of Ni(OH)₂ during hydrothermal reaction, the introduced H⁺ weakened the effect of NH₄F and accelerated the growth of Ni(OH)₂ when H₂PtCl₆ was added. We concluded that H⁺ from H₂PtCl₆ led to the formation of small nanosheets (~150 nm) of Pt/Ni(OH)₂, which gives the cataphracted morphology. Therefore, *c*-Ni(OH)₂ or *c*-Pt/Ni(OH)₂ were obtained by elaborately designing by adding HCl or NH₄OH in the hydrothermal process (see Figure 6).

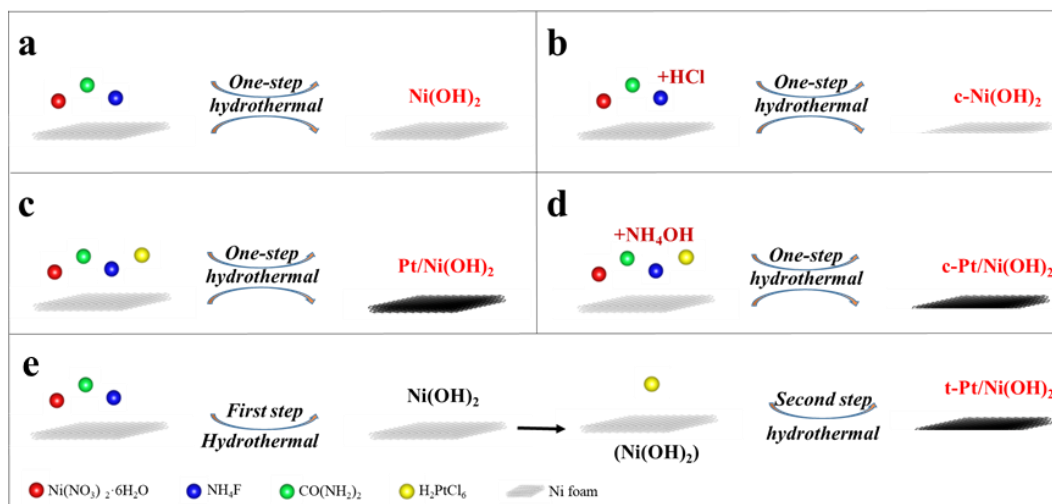


Figure 6. Schematic diagrams of (a) Ni(OH)_2 , (b) c-Ni(OH)_2 , (c) Pt/Ni(OH)_2 , (d) c-Pt/Ni(OH)_2 and (e) t-Pt/Ni(OH)_2 .

As shown in Figure 6b, c-Ni(OH)_2 with cataphracted morphology was obtained when HCl was added to the hydrothermal process. Figure 7a and 7c reveal that Ni(OH)_2 and c-Ni(OH)_2 exhibit nanosheet morphology with a size of $1\ \mu\text{m}$. Whereas, the high-magnification SEM diagram (see Figure 7d) shows the c-Ni(OH)_2 nanosheets with a length of $1\ \mu\text{m}$ are all covered by the smaller nanosheets with a length of $150\ \text{nm}$ similar to Pt/Ni(OH)_2 .

Besides, in order to form eliminate the influence of H^+ on the experiment, NH_4OH was added in the hydrothermal process in Figure 6d. The obtained sample without cataphracted structure was named as c-Pt/Ni(OH)_2 . Figure 8a and 8c display that the length of c-Pt/Ni(OH)_2 and Pt/Ni(OH)_2 nanosheets have grown to more than $2\ \mu\text{m}$. Attentively, as shown in Figure 6d, the larger nanosheets of c-Pt/Ni(OH)_2 are not covered by the smaller nanosheets.

According to other literature reports, the spontaneous oxidation-reduction reaction, driven by the difference of redox potentials of different ions and/or metals, has successfully provided a chance to fabricate Ru NPs loaded Ni(OH)_2 for electrocatalytic water splitting, due to the difference of electrochemical potentials between $\text{Ru}^{3+}/\text{Ru}^{2+}$, Ru^{2+}/Ru and Ni^{2+}/Ni [-50]. Therefore, given the electrochemical potentials of Pt^{4+}/Pt and Ni^{2+}/Ni , it is feasible to reduce Pt^{4+} (PtCl_4^{2-} from H_2PtCl_6) to Pt^0 using metal Ni derived from the Ni foam through an oxidation-reduction reaction. That could explain why larger nanosheets of Pt/Ni(OH)_2 , c-Pt/Ni(OH)_2 and t-Pt/Ni(OH)_2 grow up to more than $2\ \mu\text{m}$ long. Therefore, compared with one-step hydrothermal method, t-Pt/Ni(OH)_2 was prepared by two-step hydrothermal method in Figure 4e. Form SEM images of t-Pt/Ni(OH)_2 (Figure 9), it can see that Pt NPs ($\sim 200\ \text{nm}$) were loaded on the nanosheets. Notably, the cataphracted structure of Pt/Ni(OH)_2 prepared by one-step method can limit the size of Pt NPs to $2\sim 3\ \text{nm}$, which is in sharp contrast with t-Pt/Ni(OH)_2 . The controlled test proves the superiority of one-step hydrothermal method.

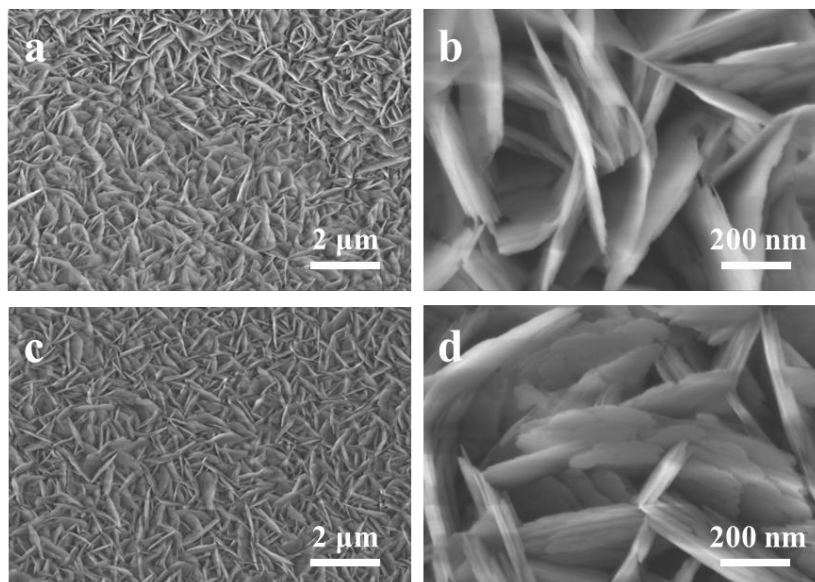


Figure 7. SEM images of (a, b) Ni(OH)₂ and (c, d) c-Ni(OH)₂.

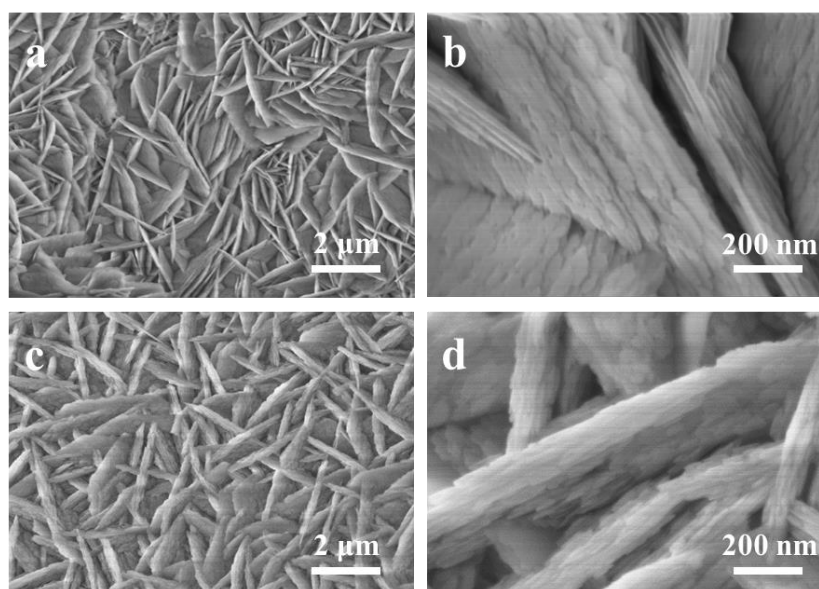


Figure 8. SEM images of (a, b) Pt/Ni(OH)₂ and (c, d) c-Pt/Ni(OH)₂.

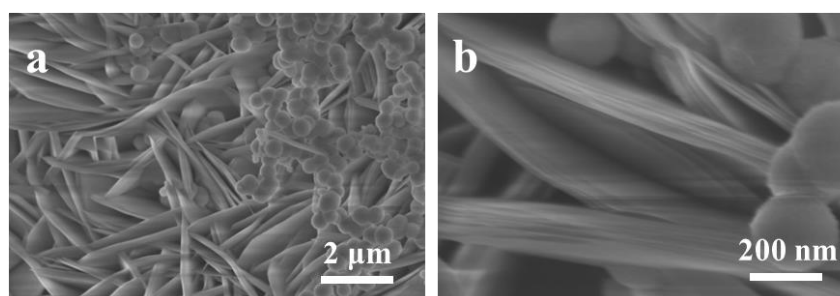


Figure 9. SEM images of (a, b) t-Pt/Ni(OH)₂.

3.6 Electrochemical Performance of $c\text{-Ni(OH)}_2$, $c\text{-Pt/Ni(OH)}_2$, $t\text{-Pt/Ni(OH)}_2$

To explore the effect of Pt/Ni(OH)₂ cataphracted structure on HER catalytic activity, the HER performance of reference samples was systematically studied in three electrode systems. As shown in Figure 10a, the overpotential of $c\text{-Ni(OH)}_2$ at the current density of 10 mA cm⁻² is 180 mV which is lower than that of Ni(OH)₂ (216 mV). Similarly, the catalytic activity of Pt/Ni(OH)₂ (34 mV) is superior to that of $c\text{-Pt/Ni(OH)}_2$ (47 mV) and $t\text{-Pt/Ni(OH)}_2$ (52 mV), which proves that the cataphracted structure formed by one-step hydrothermal method is helpful to promote the hydrogen evolution reaction. Besides, the HER performance of $c\text{-Pt/Ni(OH)}_2$ is poor than that of 3-Pt/Ni(OH)₂, which also proves 2-Pt/Ni(OH)₂ has the better HER activity than that of 3-Pt/Ni(OH)₂ benefitting from its cataphracted structure. Meanwhile, the electrochemically active surface area (ECSA) was also determined by measuring double-layer capacitance (C_{dl}). Figure 10c indicates that the C_{dl} value of $c\text{-Ni(OH)}_2$ (3.78 mF cm⁻²) exceeds that of Ni(OH)₂ (1.27 mF cm⁻²). Likewise, Pt/Ni(OH)₂ with a C_{dl} value of 72.78 mF cm⁻² exceeds $c\text{-Pt/Ni(OH)}_2$ (49.55 mF cm⁻²) and $t\text{-Pt/Ni(OH)}_2$ (37.83 mF cm⁻²), indicating that particular structure has more exposed active sites [51-52].

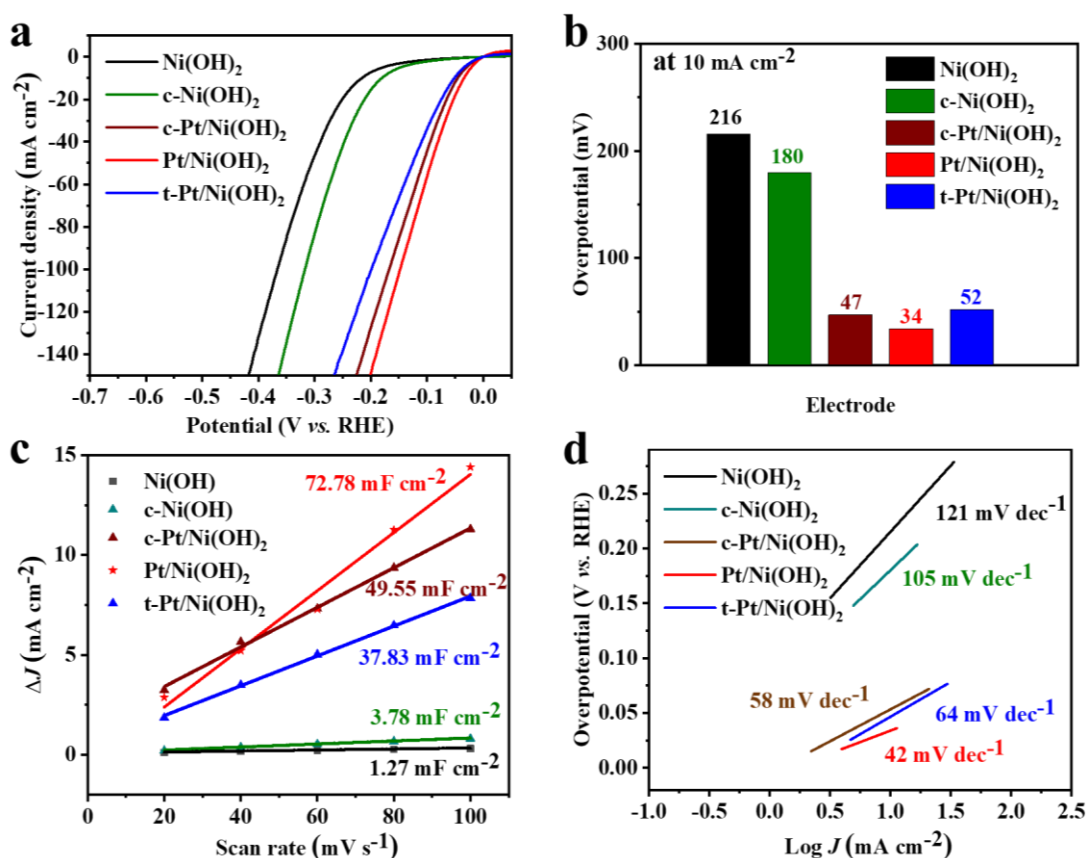


Figure 10. (a) LSV curves for Ni(OH)₂, $c\text{-Ni(OH)}_2$, Pt/Ni(OH)₂, $c\text{-Pt/Ni(OH)}_2$ and $t\text{-Pt/Ni(OH)}_2$ without iR correction at a sweep rate of 5 mV s⁻¹. (b) Overpotentials of Ni(OH)₂, $c\text{-Ni(OH)}_2$, Pt/Ni(OH)₂, $c\text{-Pt/Ni(OH)}_2$ and $t\text{-Pt/Ni(OH)}_2$ at 50 mA cm⁻² and 100 mA cm⁻². (c) Scan rate dependence of the current densities of Ni(OH)₂, $c\text{-Ni(OH)}_2$, Pt/Ni(OH)₂, $c\text{-Pt/Ni(OH)}_2$ and $t\text{-Pt/Ni(OH)}_2$. (d) Tafel plots of Ni(OH)₂, $c\text{-Ni(OH)}_2$, Pt/Ni(OH)₂, $c\text{-Pt/Ni(OH)}_2$ and $t\text{-Pt/Ni(OH)}_2$.

In Figure 10d, c-Ni(OH)₂ with a Tafel slope of 105 mV dec⁻¹ precedes Ni(OH)₂ (121 mV dec⁻¹) and the Tafel slope of Pt/Ni(OH)₂ (42 mV dec⁻¹) exceeds that of c-Pt/Ni(OH)₂ (64 mV dec⁻¹) and t-Pt/Ni(OH)₂ (66 mV dec⁻¹), which manifests c-Ni(OH)₂ and Pt/Ni(OH)₂ prominently improve the HER kinetics. It is for the reason that the cataphracted morphology favors exposure to more Ni(OH)₂ edges to greatly facilitates the water dissociation step and the 2~3 nm Pt NPs of Pt/Ni(OH)₂ synthesized by one-step hydrothermal method effectively expose the contact area of active site to actively boost the hydrogen production. The cataphracted structure enables the synergistic effect of Pt and Ni(OH)₂ to be maximized in HER. Consequently, the cataphracted structure of Pt/Ni(OH)₂ has a positive effect on promoting HER performance. The above results indicate that cataphracted structure of Pt/Ni(OH)₂ is helpful to enhance the hydrogen evolution reaction: (1) the smaller nanosheets of 150 nm long expose more active sites; (2) 2~3 nm Pt NPs are beneficial to improve the quality of active sites; (3) Pt NPs and Ni(OH)₂ nanosheets prepared by one-step hydrothermal method have a quite strong binding force which greatly enhances stability.

4. CONCLUSION

In summary, we have successfully designed one-step hydrothermal method to prepare ultralow Pt (0.35 wt %) loading cataphracted Ni(OH)₂. Cataphracted structure of Pt/Ni(OH)₂ can effectively limit the size of Pt NPs over Ni(OH)₂ nanosheets, which can provide a larger active surface area, expose more active sites and possess higher quality activity. Therefore, Pt/Ni(OH)₂ can be applied as an excellent HER catalyst in alkaline medium, which has a low overpotential (34 mV at 10 mA cm⁻²), a low Tafel slope (42 mV dec⁻¹), high ECSA (72.78 mF cm⁻²) and a long-term durability for over 40 h. Furthermore, the extremely simple one-step hydrothermal method greatly improves the utilization rate of Pt, lowers the production cost and reduces the energy consumption. This work provides a promising and cost-effective method for industrial Pt-based catalysts with low platinum load, high performance and durability.

ACKNOWLEDGEMENT

This work was supported by the National Natural Science Foundation of China (No. 11704277) and the Science and Technology Support Program of Tianjin (No. 16ZXCLGX00110 and 18ZXJMTG00300).

CONFLICTS OF INTEREST

There are no conflicts to declare.

References

1. Q. Liu, L. Xie, Z. Liu, G. Du, A.M. Asiri, X. Sun, *Chem. Commun.*, 53 (2017) 12446.
2. S. Deng, Y. Zhong, Y. Zeng, Y. Wang, Z. Yao, F. Yang, S. Lin, X. Wang, X. Lu, X. Xia, J. Tu, *Adv. Mater.*, 53 (2017) 12446.
3. X. Chen, Z. Wang, Y. Qiu, J. Zhang, G. Liu, W. Zheng, W. Feng, W. Cao, P. Hu, W. Hu, *J. Mater. Chem. A*, 4 (2016) 18060.

4. Y. Lu, W. Hou, D. Yang, Y. Chen, *Electrochim. Acta*, 307 (2019) 543.
5. J. Li, W. Hong, C. Jian, Q. Cai, *Appl. Catal., B*, 244 (2019) 320.
6. L.L. Feng, G. Yu, Y. Wu, G.D. Li, H. Li, Y. Sun, *J Am. Chem. Soc.*, 137 (2015) 14023.
7. Y. Xu, R. Wang, Y. Zheng, L. Zhang, T. Jiao, Q. Peng, Z. Liu, *Appl. Surf. Sci.*, 509 (2020) 145383.
8. H. Qin, B. Zhang, Y. Pan, X. Wang, L. Diao, J. Chen, J. Wu, E. Liu, J. Sha, L. Ma, N. Zhao, *J. Catal.*, 381 (2020) 493.
9. A. Fan, C. Qin, X. Zhang, J. Yang, J. Ge, S. Wang, X. Yuan, S. Wang, X. Dai, *J. Mater. Chem. A*, 7 (2019) 24347.
10. J. Zhu, L. Cai, X. Yin, Z. Wang, L. Zhang, H. Ma, Y. Ke, Y. Du, S. Xi, A.T.S. Wee, Y. Chai, W. Zhang, *ACS Nano*, 14 (2020) 5600.
11. A. Han, S. Jin, H. Chen, H. Ji, Z. Sun, P. Du, *J. Mater. Chem. A*, 3 (2015) 1941.
12. Q. Sun, B. Zhang, L. Diao, B. Chen, K. Song, L. Ma, F. He, *J. Mater. Chem. A*, 8 (2020) 11607.
13. P. Zhou, X. Lv, D. Xing, F. Ma, Y. Liu, Z. Wang, P. Wang, Z. Zheng, Y. Dai, B. Huang, *Appl. Catal. B*, 263 (2020) 118330.
14. Y. Ha, L. Shi, X. Yan, Z. Chen, Y. Li, W. Xu, R. Wu, *ACS Appl. Mater. Interfaces*, 11 (2019) 45546.
15. W. Fang, J. Wang, Y. Hu, X. Cui, R. Zhu, Y. Zhang, C. Yue, J. Dang, W. Cui, H. Zhao, *Electrochim. Acta*, 365 (2020) 137384.
16. L. Dai, Z.N. Chen, L. Li, P. Yin, Z. Liu, H. Zhang, *Adv. Mater.*, 32 (2020) e1906915.
17. Z. Zhang, X. Li, C. Zhong, N. Zhao, Y. Deng, X. Han, W. Hu, *Angew. Chem. Int. Ed. Engl.*, 59 (2020) 7245.
18. Y. Rao, Y. Wang, H. Ning, P. Li, M. Wu, *ACS Appl. Mater. Interfaces*, 8 (2016) 33601.
19. Q. Xu, H. Jiang, H. Zhang, Y. Hu, C. Li, *Appl. Catal., B*, 242 (2019) 60.
20. S. Sun, Y.-C. Zhang, G. Shen, Y. Wang, X. Liu, Z. Duan, L. Pan, X. Zhang, J.-J. Zou, *Appl. Catal. B*, 243 (2019) 253.
21. B. Ruqia, S.I. Choi, *Chem. Sus. Chem.*, 11 (2018) 2643.
22. E. Jung, H.-Y. Park, A. Cho, J.H. Jang, H.S. Park, T. Yu, *Appl. Catal. B*, 225 (2018) 238.
23. S. Sun, Y. Feng, L. Pan, X. Zhang, J.-J. Zou, *Appl. Catal. B*, 259 (2019) 118028.
24. X. Yu, J. Zhao, L.-R. Zheng, Y. Tong, M. Zhang, G. Xu, C. Li, J. Ma, G. Shi, *ACS Energy Lett.*, 3 (2017) 237.
25. W.C. Records, Y. Yoon, J.F. Ohmura, N. Chanut, A.M. Belcher, *Nano Energy*, 58 (2019) 167.
26. Z. Cao, Q. Chen, J. Zhang, H. Li, Y. Jiang, S. Shen, G. Fu, B.A. Lu, Z. Xie, L. Zheng, *Nat. Commun.*, 8 (2017) 15131.
27. Y. Wang, L. Chen, X. Yu, Y. Wang, G. Zheng, *Adv. Energy Mater.*, 7 (2017) 1601390.
28. L.N.T. Mai, T.C. Lam, Q.B. Bui, H.T. Nhac-Vu, *Materials Research Bulletin*, 133 (2021) 111024.
29. M. Yang, J. Zhang, W. Zhang, Z. Wu, F. Gao, *J. Alloys Compd.*, 823 (2020) 115790.
30. Y. Cao, Y. Xiahou, L. Xing, X. Zhang, H. Li, C. Wu, H. Xia, *Nanoscale*, 12 (2020) 20456.
31. J. Pan, P. Wang, P. Wang, Q. Yu, J. Wang, C. Song, Y. Zheng, C. Li, *Chem. Eng. J.*, 405 (2021) 126622.
32. X. Bao, Y. Gong, Y. Chen, H. Zhang, Z. Wang, S. Mao, L. Xie, Z. Jiang, Y. Wang, *J. Mater. Chem. A*, 7 (2019) 15364.
33. C. Wang, Y. Sun, E. Tian, D. Fu, M. Zhang, X. Zhao, W. Ye, *Electrochim. Acta*, 320 (2019) 134597.
34. L. Xie, X. Ren, Q. Liu, G. Cui, R. Ge, A.M. Asiri, X. Sun, Q. Zhang, L. Chen, *J. Mater. Chem. A*, 6 (2018) 1967.
35. S. Niu, J. Yang, H. Qi, Y. Su, Z. Wang, J. Qiu, A. Wang, T. Zhang, *J. Energy Chem*, 47 (2021) 371.
36. H. Yin, S. Zhao, K. Zhao, A. Muqsit, H. Tang, L. Chang, H. Zhao, Y. Gao, *Nat. Commun.* 6 (2015) 6430.
37. M. Xie, S. Duan, Y. Shen, K. Fang, Y. Wang, M. Lin, X. Guo, *ACS Energy Lett.*, 1 (2016) 814.
38. E.-C. Cho, C.-W. Chang-Jian, K.-C. Lee, J.-H. Huang, B.-C. Ho, R.-Z. Liu, Y.-S. Hsiao, *Chem.*

- Eng. J.*, 334 (2018) 2058.
39. W. Zhang, Y. Tang, L. Yu, X.-Y. Yu, *Appl. Catal. B*, 260 (2020) 115154.
 40. Y. Luo, X. Li, X. Cai, X. Zou, F. Kang, H.M. Cheng, B. Liu, *ACS Nano*, 12 (2018) 4565.
 41. D. Hu, X. Wang, X. Chen, Y. Wang, A.N. Hong, J. Zhong, X. Bu, P. Feng, T. Wu, *J. Mater. Chem. A*, 8 (2020) 11255.
 42. Y. Gu, Y. Wang, J. Shi, M. Yang, Y. Rui, W. An, Y. Men, *Int. J. Hydrogen Energ.*, 45 (2020) 27067.
 43. P. Zhou, G. Zhai, X. Lv, Y. Liu, Z. Wang, P. Wang, Z. Zheng, H. Cheng, Y. Dai, B. Huang, *Appl. Catal. B*, 283 (2021) 119590.
 44. K. Qi, S. Yu, Q. Wang, W. Zhang, J. Fan, W. Zheng, X. Cui, *J. Mater. Chem. A*, 4 (2016) 4025.
 45. N.H. Attanayake, S.C. Abeyweera, A.C. Thenuwara, B. Anasori, Y. Gogotsi, Y. Sun, D.R. Strongin, *J. Mater. Chem. A*, 6 (2018) 16882.
 46. K. Tang, X. Wang, Q. Li, C. Yan, *Adv. Mater.*, 30 (2018) 1704779.
 47. Z. Xing, C. Han, D. Wang, Q. Li, X. Yang, *ACS Catal.*, 7 (2017) 7131.
 48. K. Eiler, H. Krawiec, I. Kozina, J. Sort, E. Pellicer, *Electrochim. Acta*, 359 (2020) 136952.
 49. C.W. A, Y.S. A, E.T. A, D.F. A, M.Z. B, X.Z. C, W.Y. A, *Electrochim. Acta*, 320 (2019) 134597.
 50. Q.-Q. Chen, X. Yang, C.-C. Hou, K. Li, Y. Chen, *J. Mater. Chem. A*, 7 (2019) 11062.
 51. A. Wu, Y. Xie, H. Ma, C. Tian, Y. Gu, H. Yan, X. Zhang, G. Yang, H. Fu, *Nano Energy*, 44 (2018) 353.
 52. Y. Yu, X. Qiu, X. Zhang, Z. Wu, H. Wang, W. Wang, Z. Wang, H. Tan, Z. Peng, X. Guo, *Electrochim. Acta*, 299 (2019) 423